RSC Advances

PAPER

View Article Online
View Journal | View Issue

Cite this: *RSC Adv.*, 2025, **15**, 26338

DFT-based investigation of SrFAgX (X = S, Se, Te) semiconductors: structural, electronic, elastic, and optical properties for emerging optoelectronic and spintronic applications

M. A. Ghebouli,[ab] K. Bouferrache,[ac] B. Ghebouli,[d] M. Fatmi,[a] Faisal K. Alanazi*[e] and Talal M. Althagafi[f]

This study presents a comprehensive first-principles investigation of SrFAgX (X = S, Se, Te) semiconductors, focusing on the effect of chalcogen substitution on structural, elastic, electronic, and optical behavior. Using DFT-GGA calculations, we uncover systematic structure–property relationships, pressure-induced band gap tuning, and anisotropic compressibility across the series. These findings reveal how electronic and optical features can be tailored for targeted optoelectronic and spintronic applications within the generalized gradient approximation (GGA). The structural parameters, including lattice constants and internal atomic positions, show good agreement with experimental data, confirming the reliability of the computational model. The elastic constants and related mechanical moduli reveal that SrFAgS is the stiffest compound, while SrFAgSe exhibits higher flexibility, indicating tunable mechanical behavior depending on the chalcogen element. Electronic band structure analysis demonstrates that all three compounds have direct band gaps, which decrease systematically from S to Te due to enhanced orbital interactions. The calculated partial and total density of states highlight significant contributions from Ag-d and X-p states near the Fermi level, indicating strong hybridization effects. Optical properties, including dielectric function, absorption coefficient, reflectivity, refractive index, and optical conductivity, reveal systematic trends across the series, showing an enhanced optical response in SrFAgTe. These findings establish a foundation for understanding the chalcogen-dependent behavior of these materials and highlight their potential for optoelectronic, thermoelectric, and spintronic applications.

Received 6th May 2025
Accepted 14th July 2025

DOI: 10.1039/d5ra03204k

rsc.li/rsc-advances

1. Introduction

SrFAgX (X= S, Se and Te) compounds are promising semiconductors with equiatomic LaOAgS crystal structure (*P*4/*nmm* space group), characterized by remarkable properties such as ionic conductivity,[1] transparency,[2] and medium-temperature superconductivity.[3] These compounds are synthesized from mixtures of SrX, SrF_2, and Ag_2X powders, where the mixtures are either pressed into pellets and annealed under vacuum in carbon-coated silica capsules at 600–650 °C, or ground at a 1 : 1 : 1 ratio and heated at 600 °C for 48–120 hours in the presence of iodine vapor as a catalyst according to the equation: SrX + SrF_2 + Ag_2X → 2SrFAgX.[4] These materials possess a direct band gap (2.2–3.4 eV) with a unique electronic structure where the valence band edge consists primarily of Ag d-states and chalcogen p-states, while the conduction band consists of Sr s- and p-states.[5–7] They also feature low thermal conductivity (0.7–1.2 W m^{-1} K^{-1}) and exhibit a transition from insulating to semiconducting behavior with increasing temperature.[8–10] Experimental and theoretical studies have shown that the properties of these compounds change significantly under high pressure, with a phase transition from tetragonal to cubic structure at pressures exceeding 15 GPa.[11,12] These compounds are promising for various technological applications such as solar cells due to their suitable band gap,[13] transparent electronics thanks to their high transparency (>80% in the visible range),[14] photovoltaic materials because of their internal polarization,[15] and thermoelectric applications due to their low thermal conductivity.[16] Despite their promising characteristics, these compounds face challenges including difficulty in

[a]*Research Unit on Emerging Materials (RUEM), University Ferhat Abbas of Setif 1, Setif, 19000, Algeria*

[b]*Department of Chemistry, Faculty of Sciences, University of M'sila University Pole, Road Bordj Bou Arreridj, M'sila, 28000, Algeria*

[c]*Department of Physics, Faculty of Sciences, University of M'sila University Pole, Road Bordj Bou Arreridj, M'sila, 28000, Algeria*

[d]*Laboratory for the Study of Surfaces and Interfaces of Solid Materials (LESIMS), University Ferhat Abbas of Setif 1, Setif, 19000, Algeria*

[e]*Department of Physics, College of Sciences, Northern Border University, Arar 73222, Saudi Arabia. E-mail: faisal.katib.al@gmail.com*

[f]*Department of Physics, College of Sciences, Taif University, P. O. Box 11099, Taif 21944, Saudi Arabia*

preparing large, high-purity samples, limited chemical stability, and the need to improve electrical conductivity.[17] Recent studies have proposed strategies to overcome these challenges through dual transition metal doping, which improves material stability and electronic properties.[18] Recent computational studies by Xiao *et al.* have revealed strong spin–orbit coupling effects in SrFAgTe, leading to topological insulating behavior under certain conditions.[19] Advanced neutron scattering experiments by Zhao *et al.* demonstrated unique phonon transport mechanisms in these compounds, explaining their intrinsically low lattice thermal conductivity.[20] El Haj Hassan *et al.* (2024) observed novel magnetoresistance effects in SrFAgSe under high magnetic fields, suggesting potential applications in spintronic devices.[21] A groundbreaking study by Nakanishi *et al.* demonstrated efficient all-solid-state batteries using SrFAgS as a solid electrolyte with superior ionic conductivity and electrochemical stability.[22] They developed a novel low-temperature solution processing technique for SrFAgX thin films, enabling large-area fabrication with improved crystallinity and performance.[23] Furthermore, advanced first-principles calculations predicted exceptional piezoelectric properties in these materials, opening possibilities for energy harvesting applications,[24] while Amahouch *et al.* demonstrated enhanced photocatalytic hydrogen evolution using SrFAgS nanoparticles under visible light irradiation.[25] This work presents the first comprehensive theoretical investigation of the SrFAgX (X = S, Se, Te) family using DFT-GGA, focusing on how chalcogen substitution influences a wide range of material properties. While previous studies have only addressed isolated members or limited aspects of these materials, our study systematically links structural, elastic, electronic, and optical characteristics across the series. Notably, we uncover pressure-dependent band gap tuning, chalcogen-driven dielectric enhancement, and optical behavior shifts that have not been reported before. These findings offer new insights into structure–property relationships and provide a foundation for guiding future experimental and device-level research. The organization of the paper is as follows: we explain the computational method in Section 2. The computed results are presented and discussed in Section 3. We conclude the present work in Section 4.

2. Computational method

The first-principles calculations are performed using the Cambridge Serial Total Energy Package (CASTEP) code.[26] In this code, the Kohn–Sham equations are solved within the framework of density functional theory[27,28] by expanding the wave functions of valence electrons in a basis set of plane waves with kinetic energy smaller than specified cut-off energy. The presence of tightly-bound core electrons was represented by non-local ultra-soft pseudo-potentials of the Vanderbilt-type.[29] The integrations over the Brillouin zone were replaced by discrete summation over special set of *k*-points using Monkhorst–Pack scheme.[30] Plane wave cut-off energy of 660 eV and a 8 × 8 × 8 grid of Monkhorst–Pack points have been employed in this study to ensure well convergence of the computed structures and energies. For the calculation of the optical properties, which usually requires a dense mesh of uniformly distributed *k*-points, the Brillouin zone integration was performed using a 20 × 20 × 20 grid of Monkhorst–Pack points. The exchange–correlation potential was treated within GGA, developed by Perdew, Burke and Ernzerhof.[31] It should be noted that all calculations were carried out without spin polarization, since the SrFAgX (X = S, Se, Te) compounds are non-magnetic and no spin-dependent effects are expected. The structural parameters were determined using the Broyden–Fletcher–Goldfarb–Shanno (BFGS) minimization technique.[32] The tolerance for geometry optimization was set as the difference of total energy within 5×10^{-6} eV per atom, maximum ionic Hellmann–Feynman force within 0.01 eV Å^{-1} and maximum stress within 0.02 eV Å^{-3}.

3. Results and discussion

3.1 Structural properties

Table 1 presents the calculated structural and mechanical properties of SrFAgS, SrFAgSe, and SrFAgTe using DFT with the GGA approximation. The table includes lattice parameters (a, c), internal atomic positions (z_{Sr}, z_X), bulk modulus (B_0), and other elastic and mechanical constants. This section focuses on structural analysis and comparison with available experimental data. The calculated lattice constants reveal a systematic variation with chalcogen substitution. The *a*-parameter decreases from 4.054 Å (SrFAgS) to 3.919 Å (SrFAgSe) and then increases to 4.165 Å (SrFAgTe). The c-parameter shows a similar trend: 8.934 Å (SrFAgS), 10.595 Å (SrFAgSe), and 9.255 Å (SrFAgTe).

These changes reflect the increasing atomic radii from S to Te. Compared to experimental values, the relative deviations for lattice constants are as follows: SrFAgS: $\Delta a \approx 0.12\%$, $\Delta c \approx 2.38\%$, SrFAgSe: $\Delta a \approx 8.75\%$, $\Delta c \approx 10.31\%$, SrFAgTe: $\Delta a \approx 4.01\%$, $\Delta c \approx 3.53\%$. These discrepancies are within expected limits, especially for SrFAgS and SrFAgTe, and are typical of GGA-based calculations, which slightly underestimate lattice dimensions. The internal atomic coordinates (z_{Sr} and z_X) show minor variations across the three compounds, indicating structural robustness and symmetry preservation regardless of the chalcogen species. In summary, the structural properties of SrFAgX compounds exhibit consistent trends with chemical substitution and show good agreement with experimental data, particularly for SrFAgS and SrFAgTe. These findings validate the computational model and provide a solid basis for further analysis of mechanical and electronic behavior. The Fig. 1 showing the effect of pressure (0 to 40 GPa) on normalized lattice parameters for three compounds in the SrFAg family (top: SrFAgS, middle: SrFAgSe, bottom: SrFAgTe). All materials exhibit compressibility, with lattice parameters decreasing as pressure increases, notably with the *c*-axis (black line) demonstrating greater compression than the *a*-axis (blue line) across all three compounds. This indicates anisotropic compression behavior (different along various crystallographic directions). The data points (squares for a/a_0 and diamonds for c/c_0) represent experimental measurements, while the lines show fitted curves. Compression behavior varies slightly between the three compounds, with SrFAgTe displaying the most distinctive pattern. These data are significant in high-pressure

Table 1 Optimized lattice parameters (a and c, in Å), internal coordinates (z_S, z_{Sr}), bulk modulus (B_0, in GPa), bulk modulus pressure derivative (B')

	SrFAgS		SrFAgSe		SrFAgTe	
	This work	Exp.[34]	This work	Exp.[34]	This work	Exp.[34]
Lattice constant a (Å)	4.054	*4.059*	3.919	*4.165*	4.295	*4.339*
Lattice constant c (Å)	8.934	*9.152*	10.595	*9.255*	9.605	*9.594*
Sr atom position	0.157	*0.153*	0.165	*0.150*	0.136	*0.135*
X atom position	0.691	*0.694*	0.680	*0.695*	0.701	*0.697*
B (GPa)	75.78		57.66		62.47	
B'	4.729		4.385		4.461	
C_{11} (GPa)	128.12		*119.66*		102.91	
C_{33} (GPa)	89.51		*85.05*		63.27	
C_{44} (GPa)	41.28		*22.83*		31.53	
C_{66} (GPa)	29.95		*36.40*		21.91	
C_{12} (GPa)	44.45		*51.14*		25.94	
C_{13} (GPa)	56.48		*29.42*		40.69	
B* (GPa)	72.15		*57.32*		52.26	
B'*	4.686		*4.501*		5.402	

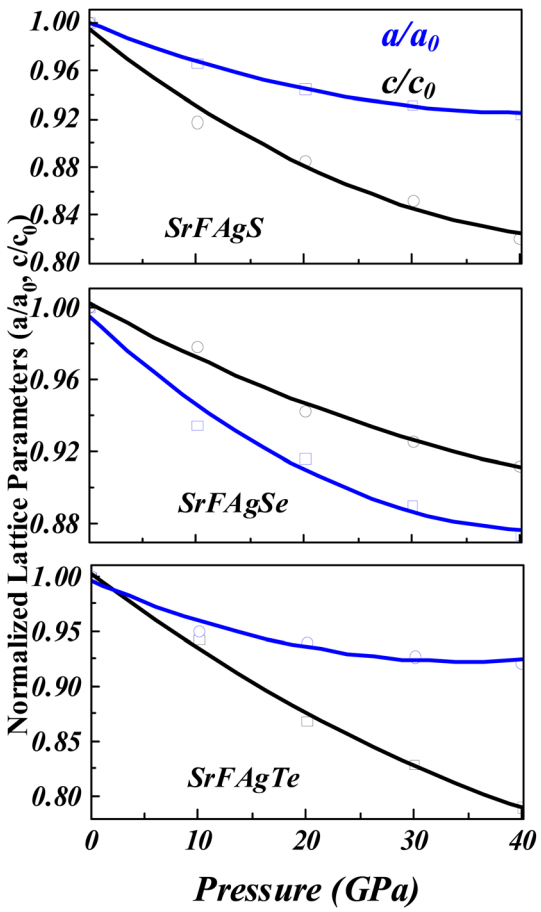

Fig. 1 Pressure dependent normalized lattice parameters (a/a_0 and c/c_0) for SrFAgS, SrFAgSe, and SrFAgTe compounds, showing anisotropic compressibility with greater contraction along the c-axis than the a-axis under increasing pressure.

crystallographic studies for understanding the structural response of strontium-fluoride–silver chalcogenide compounds (S, Se, Te variants) under increasing pressure conditions, demonstrating how these materials compress anisotropically throughout the series.

3.2 Elastic properties

3.2.1 Elastic constants. The elastic properties of SrFAgS, SrFAgSe, and SrFAgTe compounds show clear differences in their mechanical behavior. The bulk modulus (B) is highest for SrFAgS (75.78 GPa), indicating it has the greatest resistance to compression, followed by SrFAgTe (62.47 GPa), and then SrFAgSe (57.66 GPa), which is the least resistant. The pressure derivative of the bulk modulus (B') is very similar among the compounds (around 4.4–4.7), suggesting a comparable response to increasing pressure. Regarding the elastic constants, SrFAgS exhibits the highest values for C_{11} and C_{33}, meaning it is the stiffest along the crystal axes. For the shear constants (C_{44} and C_{66}), SrFAgS has the highest C_{44}, while SrFAgSe has the highest C_{66}, reflecting greater shear flexibility in certain directions for SrFAgSe. The inter-axial constants (C_{12} and C_{13}) also indicate that SrFAgSe is more flexible transversely. The calculated bulk modulus (B') supports these findings, with SrFAgS remaining the stiffest, followed by SrFAgTe and then SrFAgSe. Overall, SrFAgS is the stiffest and least flexible, SrFAgSe demonstrates higher flexibility in some properties, and SrFAgTe is intermediate. These differences are attributed to the type of X atom (S, Se, or Te) and its effect on the crystal structure and atomic bonding, making the choice of compound dependent on the application's requirements for rigidity or flexibility. The flexibility of the SrFAgX compounds was evaluated based on the calculated elastic constants. In particular, lower values of shear moduli (C_{44}, C_{66}) and inter-axial elastic constants (C_{12}, C_{13}) in SrFAgSe, compared to SrFAgS, indicate higher mechanical flexibility. These parameters are standard indicators of a material's resistance to deformation and are widely used in first-principles studies to assess elastic behavior in the absence of experimental mechanical data.

Regarding stability criteria for these tetragonal compounds, mechanical stability requires elastic constants to satisfy Born

criteria for tetragonal crystals, such as:[33] $C_{11} > 0$, $C_{33} > 0$, $C_{44} > 0$, $C_{66} > 0$, $C_{11} > C_{12}$ and $2C_{13}^2 < C_{33} \times (C_{11} + C_{12})$ based on elastic constants, all these conditions appear to be met, indicating mechanical stability of SrFAgS, SrFAgSe, and SrFAgTe phases.

3.3 Electronic properties

3.3.1 Band structure. The Fig. 2 presents the electronic band structures of SrFAgS, SrFAgSe, and SrFAgTe compounds, with energy (in eV) plotted vertically and momentum paths in the Brillouin zone plotted horizontally. All three materials show multiple electronic bands, with the Fermi level is set to zero and aligned with the top of the valence band. The energy range is limited to −4 eV to +8 eV to emphasize the band gap region. As shown in Fig. 2, all compounds exhibit direct band gaps. The reduction in gap from SrFAgS to SrFAgTe is consistent with increased atomic size and enhanced orbital overlap, which facilitates better charge carrier mobility. This behavior supports the use of SrFAgTe in applications requiring stronger electrical conductivity and optical absorption in lower energy ranges. SrFAgS exhibits the largest band gap, indicating it is the most insulating among the three. The band gap in these materials appears to be indirect, as the top of the valence band and the bottom of the conduction band are not aligned at the same *k*-point. High-symmetry points such as *Z*, *A*, *M*, *Γ*, *R*, and *X* represent critical directions in the Brillouin zone, providing insights into the electronic transitions and carrier dynamics. SrFAgTe, with the smallest band gap, is predicted to have the highest conductivity and may even show semimetallic behavior. In contrast, SrFAgS, with its wide gap, is more suitable for insulating applications. The gradual reduction of the band gap from S to Te highlights the tunability of electronic properties in these materials by chemical substitution. This tunability is essential for designing materials for specific electronic or optoelectronic applications. Overall, the band structure analysis reveals a clear relationship between chemical composition and electronic behavior in the SrFAgX (X = S, Se, Te) family. The Fig. 3, illustrate how the electronic band gap changes with applied pressure. For SrFAgS, the band gap increases steadily as the pressure rises, indicating a continuous enhancement of its insulating properties. In contrast, both SrFAgSe and SrFAgTe exhibit a maximum band gap at certain pressures; beyond this point, the band gap decreases with further pressure increase. This behavior demonstrates the sensitivity of these compounds to external pressure and highlights the possibility of tuning their electronic properties through pressure control. The

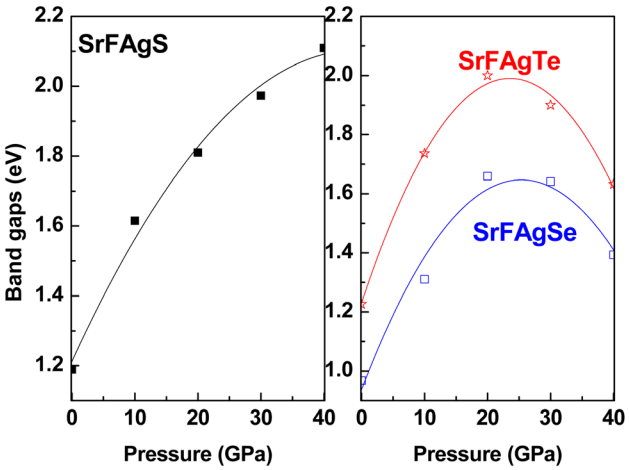

Fig. 3 Evolution of electronic band gaps of SrFAgX compounds under applied pressure up to 40 GPa, revealing a monotonic increase for SrFAgS and non-monotonic behavior for SrFAgSe and SrFAgTe.

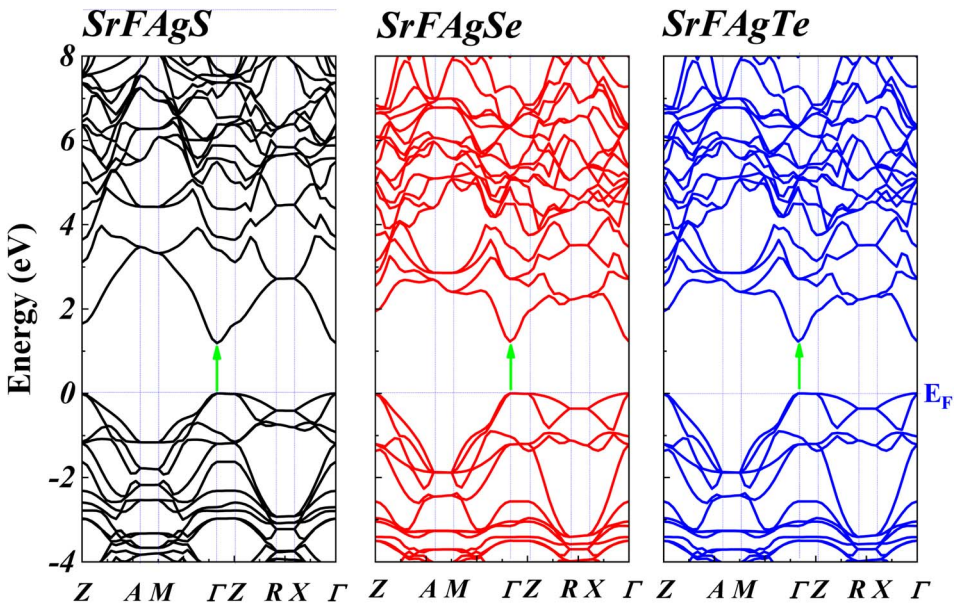

Fig. 2 Electronic band structures of SrFAgX (X = S, Se, Te) along high-symmetry directions, indicating direct band gaps that decrease from S to Te due to enhanced orbital overlap and chalcogen substitution effects.

distinct response of each compound to pressure variation also suggests their potential for use in various technological applications, especially where stability or tunability of the band gap is required.

3.3.2 Partial and total density of state. Analysis of the partial and total density of state of SrFAgX (X = S, Se, Te) compounds are show in Fig. 4, reveals systematic evolution across the chalcogen series. The band structure diagrams display complex dispersions with multiple crossings, particularly near the Fermi level, with band gap narrowing observed when progressing from S to Se to Te. This trend is further confirmed by the projected density of states (PDOS) analysis, which decomposes contributions from individual atomic orbitals. The PDOS shows significant chalcogen p-orbital contributions near the valence band maximum, while Ag d-orbitals feature prominently across specific energy regions, suggesting substantial p-d hybridization effects. This hybridization plays a central role in defining the electronic structure near the Fermi level and is directly linked to the observed optical transitions, therefore, the PDOS analysis not only confirms the band structure results but also explains the origin of enhanced optical activity in heavier chalcogen compounds such as SrFAgTe. Strontium and fluorine contributions are primarily located at deeper energy levels. The unique combination of alkaline earth, halogen, transition metal, and chalcogen elements creates opportunities for band structure engineering through compositional tuning. The systematic changes in electronic properties make these materials promising candidates for optoelectronic applications, where precise band gap control is essential. These theoretical findings provide substantial insight into the chalcogen-dependent electronic behavior, establishing a foundation for future experimental verification and potential applications in photovoltaics or topological materials research.

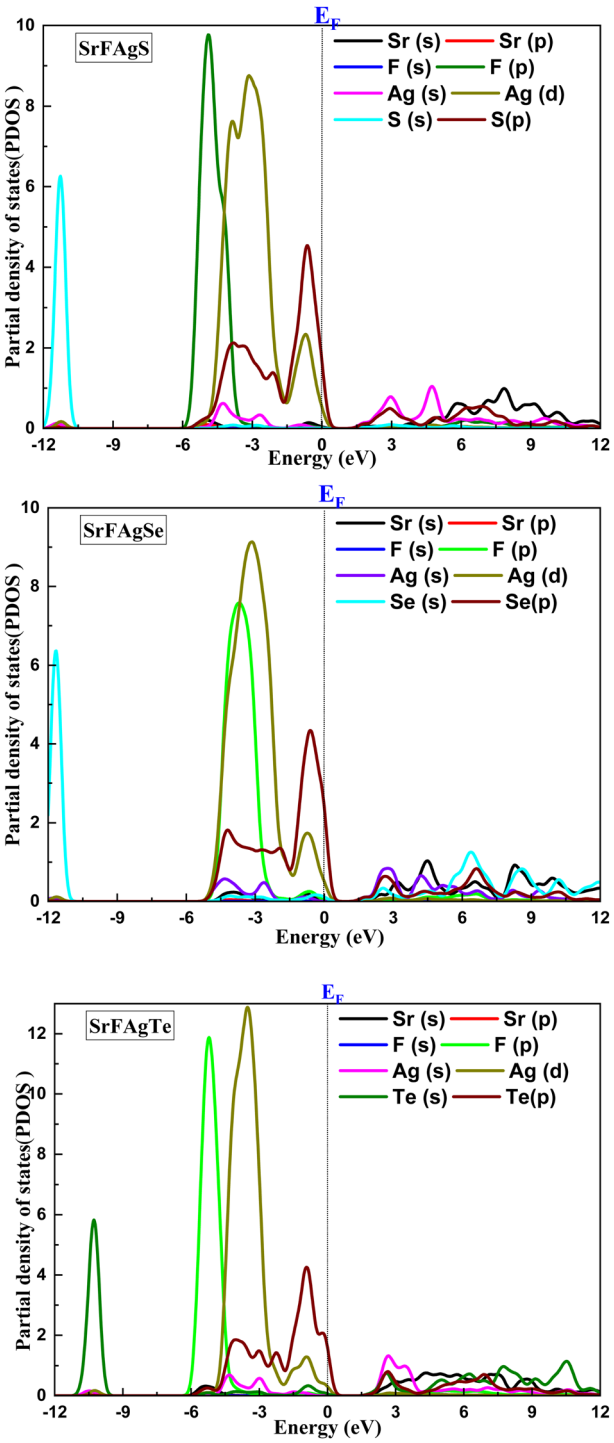

Fig. 4 Partial density of states (PDOS) for SrFAgX compounds, illustrating strong Ag-d and X-p orbital hybridization near the Fermi level, which contributes to the observed electronic properties.

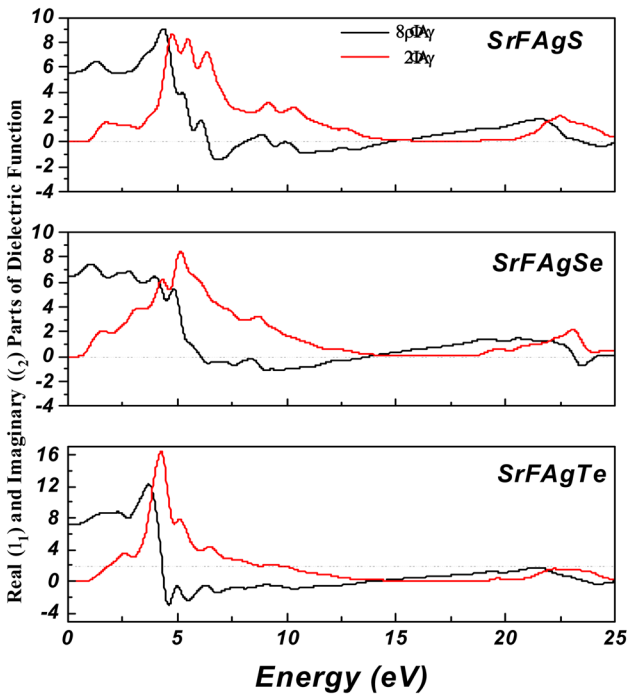

Fig. 5 Real (ε_1) and imaginary (ε_2) parts of the complex dielectric function for SrFAgS, SrFAgSe, and SrFAgTe as functions of photon energy, highlighting enhanced optical response and static dielectric constant in SrFAgTe compared to its lighter counterparts.

3.4 Optical properties

3.4.1 Dielectric function. Fig. 5 displays the dielectric functions for SrFAgX (X = S, Se, Te) compounds, showing both the real $\varepsilon_{(1)}$ and imaginary $\varepsilon_{(2)}$ components plotted against energy in eV. The figure provides insight into the electronic transitions and polarization response of the SrFAgX compounds across different energy regions. For SrFAgS (top panel), the real part (black line) shows oscillations around 0–10 eV with notable peaks, while the imaginary part (red line) exhibits strong absorption features between 5 and 10 eV, indicating electronic transitions in this energy range. The middle panel for SrFAgSe shows similar characteristics but with slightly modified peak positions and intensities compared to the sulfur compound, suggesting systematic changes in optical properties with chalcogen substitution. The bottom panel for SrFAgTe reveals the most dramatic differences, with significantly higher amplitude in both components and a prominent sharp peak around 5 eV. The *y*-axis scale extends to higher values (reaching 16), indicating stronger optical response in the tellurium compound. This strong dielectric response in SrFAgTe, especially in the 4–10 eV range, is attributed to its narrower band gap and higher density of states near the Fermi level, which facilitates interband transitions. The systematic evolution across the chalcogen series demonstrates how optical response can be tuned through compositional engineering. The presence of significant peaks in the visible and UV range suggests potential applications in optoelectronic devices where specific optical characteristics are required. The static dielectric constant $\varepsilon_{(1)}$ at $E = 0$ eV increases systematically from approximately 6 for SrFAgS to 8 for SrFAgSe and 9 for SrFAgTe. This increasing trend in static dielectric values correlates inversely with the band gap reduction observed in the band structure calculations, confirming the expected relationship between dielectric response and band gap in semiconductors. The combination of alkaline earth (Sr), halogen (F), transition metal (Ag), and chalcogen (S, Se, Te) elements enables strong orbital hybridization and rich electronic interactions. This interplay supports band gap tuning and dielectric enhancement, which are valuable for optoelectronic and thermoelectric applications.[35] These features indicate that SrFAgTe is particularly promising for optoelectronic devices requiring high dielectric activity in the visible and ultraviolet spectral ranges. These theoretical findings provide substantial insight into the chalcogen-dependent electronic and optical behavior, establishing a foundation for future experimental verification and potential applications in photovoltaics or optoelectronic devices where precise control of both electronic and optical properties is essential.

3.4.2 Absorption, reflectivity and loss function. Fig. 6 presents the absorption spectra, reflectivity, and energy loss function for SrFAgX (X = S, Se, Te) compounds as functions of photon energy (eV). The absorption spectra (top panel) reveal two major regions of optical activity: a broad absorption band from approximately 5–15 eV and a sharper, more intense peak around 25 eV. Among the compounds, SrFAgSe (red line) exhibits the most intense absorption peak, which occurs in the high-energy region between 20 and 25 eV, reaching nearly 420 000 units. This strong absorption indicates intense interband transitions characteristic of this composition. The reflectivity data (middle panel) show similar overall trends across the series, with multiple peaks appearing below 15 eV followed by a dip, then a second peak around 25 eV. Notably, SrFAgTe displays the highest reflectivity, peaking at approximately 0.5 near 15 eV.

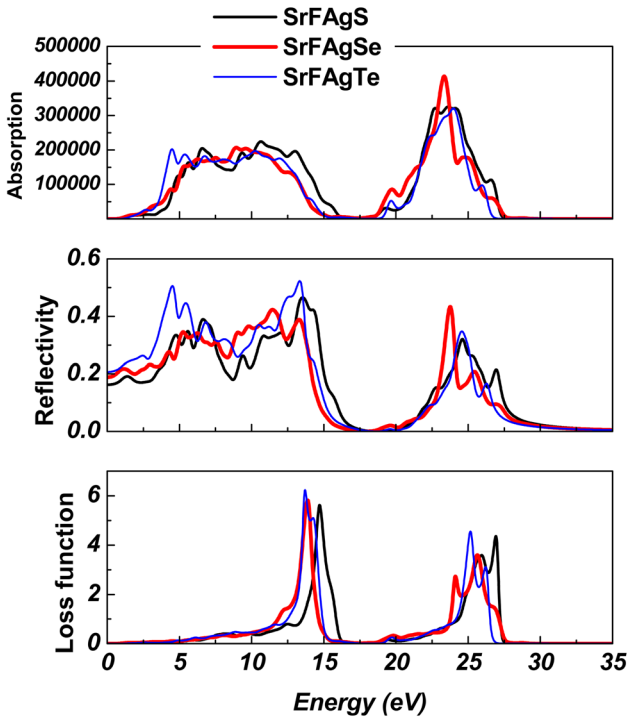

Fig. 6 Absorption spectra, reflectivity, and energy loss function of SrFAgX compounds, showing stronger absorption in the visible-UV range and higher energy loss peaks in SrFAgTe, indicating stronger plasmonic activity.

The energy loss function (bottom panel), which provides insight into collective electron excitations (plasmons), shows two strong peaks: the first near 15 eV and the second around 25 eV. The first energy loss peak in SrFAgTe is the most intense among the series, indicating stronger plasmonic activity, which is desirable for applications in energy dissipation and shielding.

The main absorption peaks observed in SrFAgTe at 5–8 eV also correlate well with its enhanced dielectric function and higher optical conductivity, confirming its superior optical performance.

These optical properties demonstrate that the substitution of heavier chalcogens leads to enhanced optical response at lower photon energies, in agreement with the narrowing band gap and increasing dielectric constant trends discussed earlier.

3.4.3 Refractive index and optical conductivity. Fig. 7 illustrates the properties of SrFAgS, SrFAgSe, and SrFAgTe compounds in terms of refractive index and optical conductivity as a function of energy. In the upper plot, it is observed that all compounds start with a relatively high refractive index at low energies (at 0 eV), where the refractive index is approximately

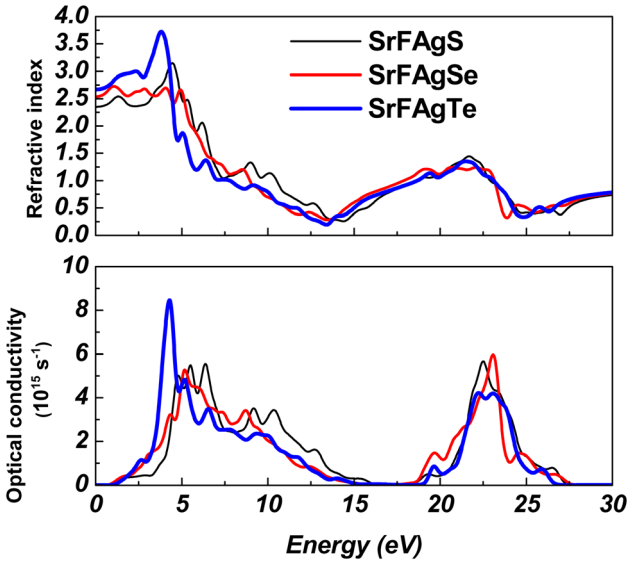

Fig. 7 Refractive index and optical conductivity of SrFAgX compounds as functions of photon energy, demonstrating stronger interband transitions and higher optical conductivity peaks in SrFAgSe and SrFAgTe.

3.0 for SrFAgS, 2.9 for SrFAgSe, and 2.8 for SrFAgTe. The optical conductivity at this energy is nearly zero for all compounds. As the energy increases, the refractive index gradually decreases and stabilizes at low values above 20 eV. SrFAgS (black curve) shows the highest refractive index at low energies compared to the other two compounds. In the lower plot, the optical conductivity displays two prominent peaks: the first around 4 eV and the second between 20 and 25 eV. SrFAgSe (red curve) exhibits the highest peak in optical conductivity, indicating strong electronic transitions in this compound. Generally, the optical conductivity is very low at extremely low energies, then increases significantly at the two main peaks. There is also a similarity in the general behavior of the three compounds, with slight differences in the maximum values.

The higher refractive index at low energy, particularly in SrFAgS, is consistent with its wider band gap and stronger polarizability, while the reduced values in SrFAgTe reflect its enhanced free carrier contribution and narrower gap.

The optical conductivity trends support the electronic band structures, where increased state density and interband transitions in SrFAgSe contribute to its strong optical activity.

These results reflect differences in the electronic structure and crystal lattice of the compounds and their impact on the optical properties.

Such behavior suggests that tuning the chalcogen element allows control over transparency and light–matter interaction, making these compounds suitable for photonic coatings, transparent conductors, or wavelength-selective optoelectronic devices.

The curves highlight the importance of these materials in optical and electronic applications, especially in fields that require materials with specific optical responses within certain energy ranges.

4. Conclusion

In summary, this study provides a detailed theoretical analysis of the SrFAgX (X = S, Se, Te) semiconductors, revealing how chalcogen substitution influences their structural, elastic, electronic, and optical properties. The results demonstrate a clear trend in lattice parameters and mechanical stiffness across the series, with SrFAgS being the most rigid and SrFAgSe the most flexible. The electronic structure calculations confirmed the presence of direct band gaps that decrease systematically from S to Te, accompanied by strong Ag–X hybridization near the Fermi level. Optical analysis showed enhanced dielectric and absorption properties in SrFAgTe, indicating potential for tailored optoelectronic performance. Additionally, pressure-dependent simulations revealed tunable band gap behavior and anisotropic compressibility. These findings not only deepen the understanding of SrFAgX materials but also highlight their suitability for targeted applications in optoelectronic, thermoelectric, and spintronic devices. Future experimental studies and material engineering efforts are encouraged to validate these predictions and optimize performance for real-world applications. Future experimental studies and material engineering efforts are encouraged to validate these predictions and optimize performance for real-world applications.

Data availability

Data underlying the results presented in this paper are not publicly available at this time but may be obtained from the corresponding author (fatmimessaud@yahoo.fr) upon reasonable request.

Author contributions

Data curation: M. A. Ghebouli, B. Ghebouli, analysis: K. Bouferrache, Faisal K. Alanazi, Talal M. Althagafi, methodology, validation: M. Fatmi.

Conflicts of interest

The authors declare that they have no conflict of interest.

Acknowledgements

The authors extend their appreciation to the Deanship of Scientific Research at Northern Border University, Arar, KSA for funding this research work through the project number NBU-FFR-2025-310-17.

References

1 D. O. Charkin, A. V. Urmanov and S. M. Kazakov, Preparation and crystal structures of novel LaOAgS-type copper and silver fluoride chalcogenides, *J. Alloys Compd.*, 2012, **516**, 134–138, DOI: 10.1016/j.jallcom.2011.11.151.

2 B. Doumi, A. Mokaddem, L. Temimi, N. Beldjoudi, M. Elkeurti, F. Dahmane, A. Sayede, A. Tadjer and M. Ishak-Boushaki, First-principle investigation of half-metallic ferromagnetism in octahedrally bonded Cr-doped rock-salt SrS, SrSe, and SrTe, *Eur. Phys. J. B*, 2015, **88**, 1–9, DOI: 10.1140/epjb/e2015-50746-9.

3 K. Biswas, J. He, Q. Zhang, G. Wang, C. Uher, V. P. Dravid and M. G. Kanatzidis, Investigation of the thermoelectric properties of the PbTe-SrTe system, *MRS Online Proc. Libr.*, 2010, **1267**, 1–6, DOI: 10.1557/PROC-1267-DD06-05.

4 M. N. Buslaeva, K. T. Dudnikova and O. Y. Samoilov, Dependence of salting out on near hydration of salting-out anion, *J. Struct. Chem.*, 1969, **10**(1), 5–8, DOI: 10.1007/BF00751944.

5 L. Abtin and G. Springholz, Stabilization of PbSe quantum dots by ultrathin EuTe and SrTe barrier layers, *Appl. Phys. Lett.*, 2008, **93**, 163102, DOI: 10.1063/1.3000386.

6 S. Labidi, H. Meradji, M. Labidi, S. Ghemid, S. Drablia and F. E. H. Hassan, First principles calculations of structural, electronic and thermodynamic properties of SrS, SrSe, SrTe compounds and $SrS_{1-x}Se_x$ alloy, *Phys. Procedia*, 2009, **2**(3), 1205–1212, DOI: 10.1016/j.phpro.2009.11.083.

7 Y. J. Kim, L. D. Zhao, M. G. Kanatzidis and D. N. Seidman, Analysis of nanoprecipitates in a Na-doped PbTe–SrTe thermoelectric material with a high figure of merit, *ACS Appl. Mater. Interfaces*, 2017, **9**(26), 21791–21797, DOI: 10.1021/acsami.7b04098.

8 R. Khenata, H. Baltache, M. Rérat, M. Driz, M. Sahnoun, B. Bouhafs and B. Abbar, First-principle study of structural, electronic and elastic properties of SrS, SrSe and SrTe under pressure, *Phys. B*, 2003, **339**(4), 208–215, DOI: 10.1016/j.physb.2003.07.003.

9 S. Kapoor, P. Bhardwaj and N. Yaduvanshi, Study of the phase transition phenomenon in SrTe under pressure, *Adv. Phys. Theo. Appl.*, 2015, **45**, 92.

10 J. Androulakis, I. Todorov, J. He, D. Y. Chung, V. Dravid and M. Kanatzidis, High-performance nanostructured thermoelectric PbSe–SrTe, *J. Am. Chem. Soc.*, 2011, **133**(28), 10920–10927, DOI: 10.1021/ja203022c.

11 D. Rached, M. Rabah, N. Benkhettou, B. Soudini and H. Abid, Electronic and structural properties of strontium chalcogenides SrS, SrSe and SrTe, *Phys. Status Solidi B*, 2004, **241**(11), 2529–2537, DOI: 10.1002/pssb.200402053.

12 L. Shi, Y. Duan, X. Yang and L. Qin, Structural stabilities, electronic, elastic and optical properties of SrTe under pressure: a first-principles study, *Phys. B*, 2011, **406**(2), 181–186, DOI: 10.1016/j.physb.2010.10.038.

13 Y. Xiao, Y. Su, R. Mittal, T. Chatterj, T. Hansen, S. Price, C. M. N. Kumar, J. Persson, S. Matsuishi, Y. Inoue, H. Hosono and T. Bruecke, Neutron diffraction study of phase transitions and thermal expansion of SrFeAsF, *Phys. Rev. B: Condens. Matter Mater. Phys.*, 2010, **81**, 094523, DOI: 10.1103/PhysRevB.81.094523.

14 S. Haireche, S. Douakh, M. Elbaa, M. Bouchenafa and K. Meliani, Influence of phase transition on the mechanical and optical properties of SrSe and SrTe compounds *via ab initio* calculations, *Phys. B*, 2025, **696**, 416610, DOI: 10.1016/j.physb.2024.416610.

15 C. Gayner and N. Nandihalli, Enhancement of thermoelectric performance of PbTe by embedding NaCl, *Materialia*, 2020, **14**, 100912, DOI: 10.1016/j.mtla.2020.100912.

16 H. G. Zimmer, H. Winzen and K. Syassen, High-pressure phase transitions in CaTe and SrTe, *Phys. Rev. B: Condens. Matter Mater. Phys.*, 1985, **32**(6), 4066, DOI: 10.1103/PhysRevB.32.4066.

17 L. D. Zhao, X. Zhang, H. Wu, G. Tan, Y. Pei, Y. Xiao, C. Chang, D. Wu, H. Chi, L. Zheng, S. Gong, C. Uher, J. He and M. G. Kanatzidis, Enhanced thermoelectric properties in the counter-doped SnTe system with strained endotaxial SrTe, *J. Am. Chem. Soc.*, 2016, **138**(7), 2366–2373, DOI: 10.1021/jacs.5b13276.

18 J. Zeroual, S. Labidi, H. Meradji, M. Labidi and F. E. Haj Hassan, *Ab initio* calculations of fundamental properties of $SrTe_{1-x}O_x$ alloys, *Bull. Mater. Sci.*, 2016, **39**, 827–835, DOI: 10.1007/s12034-016-1189-8.

19 Y. Xiao-Cui, H. Ai-Min, Y. Jie, H. Yong-Hao, P. Gang, G. Chun-Xiao and Z. Guang-Tian, Theoretical prediction for structural stabilities and optical properties of SrS, SrSe and SrTe under high pressure, *Chin. Phys. Lett.*, 2008, **25**(5), 1807, DOI: 10.1088/0256-307X/25/5/077.

20 L. D. Zhao, H. J. Wu, S. Q. Hao, C. I. Wu, X. Y. Zhou, K. Biswas, J. Q. He, T. P. Hogan, C. Uher, C. Wolverton, V. P. Dravid and M. G. Kanatzidis, All-scale hierarchical thermoelectric: MgTe in PbTe facilitates valence band convergence and suppresses bipolar thermal transport for high performance, *Energy Environ. Sci.*, 2013, **6**, 3346–3355, DOI: 10.1039/c3ee42187b.

21 F. El Haj Hassan, H. Akbarzadeh, S. Hashemifar and A. Mokhtari, Structural and electronic properties of matlockite MFX (M = Sr, Ba, Pb; X = C1, Br, I) compounds, *J. Phys. Chem. Solids*, 2024, **65**(11), 1871–1878, DOI: 10.1016/j.jpcs.2004.07.002.

22 Y. Nakanishi, T. Ito, Y. Hatanaka and G. Shimaoka, Preparation and luminescent properties of SrSe:Ce thin films, *Appl. Surf. Sci.*, 1993, **65**, 515–519, DOI: 10.1016/0169-4332(93)90712-K.

23 D. Varshney, N. Kaurav, R. Kinge and R. K. Singh, High pressure structural (B1–B2) phase transition and elastic properties of II–VI semiconducting Sr chalcogens, *Comput. Mater. Sci.*, 2008, **41**(4), 529–537, DOI: 10.1016/j.commatsci.2007.05.009.

24 M. Souadkia, B. Bennecer, F. Kalarasse and A. Mellouki, *Ab initio* calculation of vibrational and thermodynamic properties of SrX (S, Se, Te) in the B1 (NaCl) and B2 (CsCl) structures, *Comput. Mater. Sci.*, 2011, **50**(5), 1701–1710, DOI: 10.1016/j.commatsci.2010.12.031.

25 A. Amahouch, R. Laamara and L. B. Drissi, Stability of ferromagnetism in diluted magnetic $Sr_{1-x}Cr_xX$ (X = S, Se and Te) semiconductor doped by Cr under Hubbard correction and strain effect, *Phys. Scr.*, 2025, **100**, 065924, DOI: 10.1088/1402-4896/add21d.

26 L. Krache, M. A. Ghebouli, B. Ghebouli, M. Fatmi, T. Chihi and S. I. Ahmed, Structural, Elastic, Electronic and Optical Properties Study of Hexahalometallate Single Crystals X_2SnBr_6 (X = Rb, Cs), *Acta Phys. Pol. A*, 2023, **143**, 3–11, DOI: **10.12693/AphysPolA.143.30**.

27 R. Boudissa, Z. Zerrougui, M. A. Ghebouli, K. Bouferrache, L. Krache, T. Chihi, B. Ghebouli, A. Habila, M. Fatmi and M. Sillanpää, Prediction study of structural, electronic and optical properties of $4C_{16}H_{10}Br_2O_2$ bis(*m*-bromobenzoyl) methane crystals, *Biochem. Biophys. Rep.*, 2024, **37**, 101601, DOI: **10.1016/j.bbrep.2023.101601**.

28 B. Ghebouli, M. A. Ghebouli, M. Fatmi, N. Bouarissa, M. Benkerri and I. A. Ibrahim, Structural, elastic and electronic properties for M_2XC (M = Ti and Cr, X = Ga and Al) phases from *ab initio* calculations, *Acta Metall. Sin. (Engl. Lett.)*, 2011, **24**(4), 255–270, DOI: **10.11890/1006-7191-114-255**.

29 B. Ghebouli, M. A. Ghebouli and M. Fatmi, Structural, elastic, electronic, optical and thermal properties of cubic perovskite $CsCdF_3$ under pressure effect, *Eur. Phys. J.: Appl. Phys.*, 2011, **53**, 30101, DOI: **10.1051/epjap/2010100318**.

30 B. Ghebouli, M. Fatmi, M. A. Ghebouli, H. Choutri, L. Louail, T. Chihi, A. Bouhemadou and S. Bin-Omran, Theoretical study of the structural, elastic, electronic and optical properties of $XCaF_3$ (X= K and Rb), *Solid State Sci.*, 2015, **43**, 9–14, DOI: **10.1016/j.solidstatesciences.2015.03.009**.

31 B. Ghebouli, M. A. Ghebouli, M. Fatmi and M. Benkerri, First-principles calculations of structural, elastic, electronic and optical properties of XO (X = Ca, Sr and Ba) compounds under pressure effect, *Mater. Sci. Semicond. Process.*, 2010, **13**(2), 92–101, DOI: **10.1016/j.mssp.2010.04.001**.

32 K. Bouferrache, M. A. Ghebouli, B. Ghebouli, M. Fatmi and S. I. Ahmed, Correction: Organic–inorganic hexahalometalate-crystal semiconductor K_2 (Sn, Se, Te) Br_6 hybrid double perovskites for solar energy applications, *RSC Adv.*, 2025, **15**(22), 17377, DOI: **10.1039/D5RA00862J**.

33 M. Born and K. Huang, *Dynamical Theory of Crystal Lattices*, Clarendon, Oxford, 1954.

34 D. O. Charkin, A. V. Urmanov and S. M. Kazakov, Preparation and crystal structures of novel LaOAgS-type copper and silver fluoride chalcogenides, *J. Alloys Compd.*, 2012, **516**, 134–138, DOI: **10.1016/j.jallcom.2011.11.151**.

35 R. Woods-Robinson, Y. Han, H. Zhang, T. Ablekim, I. Khan, K. A. Persson and A. Zakutayev, Wide band gap chalcogenide semiconductors, *Chem. Rev.*, 2020, **120**(9), 4007–4055, DOI: **10.1021/acs.chemrev.9b00600**.